Paper No.
08295

NACE INTERNATIONAL CORROSION 2008 CONFERENCE & EXPO

CORROSION MONITORING OF A WATER BASED ROLLING FACILITY WITH COUPLED MULTIELECTRODE ARRAY SENSORS AND THE CORRELATIONS WITH OTHER PROCESS VARIABLES: CONDUCTIVITY, PH, TEMPERATURE, DISSOLVED OXYGEN AND CORROSION POTENTIAL

Raymond Colbert
Ronald Reich
Alcoa Technical Center
Aluminum Company of America
Alcoa Center, Pennsylvania 15069

Abstract

Coupled multielectrode array sensors[1-5](CMAS) with multielectrode corrosion analyzer and temperature monitoring capability were used along with an Isfet type pH probe, a process contact conductivity probe, and dissolved oxygen probe to monitor data over one year in an Alcoa rolling mill coolant system. During this time several excursions of various parameters occurred, indicating chemical and possible electrical causes of corrosion. A CMAS type crevice type probe was also used to investigate crevice corrosion (a common problem on piping and fixtures coming in external contact with the mill coolant) and was used to determine material/engineering recommendations for prevention of corrosion in rolling mills.

INTRODUCTION

The objective of this project was to develop a corrosion monitoring program to continuously measure corrosion and causative parameters in a water-based coolant system of an aluminum rolling facility. A corrosion monitor with multi electrode probes (CMAS) and temperature monitoring capability, with a recording computer, an Isfet type pH probe, a contact type conductivity probe, and a dissolved oxygen probe, was assembled and installed in the coolant house and process piping. This paper describes the monitoring system and the results.

INSTRUMENTATION AND SYSTEM SETUP

Probes and Instrumentation

Coupled multielectrode array sensors[1-5](CMAS) were used for the measurements of localized corrosion.

- S-36 nanoCorr [(1)] multielectrode corrosion analyzer
- 18-electrode probe for Type 1018 carbon steel (UNS G10180)
- 18-electrode combination probe with 9 electrodes for Type 304L stainless steel (UNS S30403) and 9 electrodes for Type 1018 carbon steel (UNS G10180)
- Creviced 18-electrode combination probe with 9 electrodes for Type 304L stainless steel and 9 electrodes for Type 1018 carbon steel

[(1)]Corr Instruments LLC. San Antonio Texas

All electrodes were 1.0 mm in diameter and flush-mounted in an epoxy. The combination probes were essentially two sensors built in one probe (Figure 1). During the measurements, half of the electrodes that were made of the same metal were coupled together as the first sensor and the half of the electrodes that were made of the second metal were coupled together as the second sensor; the coupling joints of the two types of sensors were separated. A typical creviced probe is shown in Figure 2. Two layers of acid-free paper were used between the crevice former and the sensor electrode. The corrosion analyzer could be used with two of the above probes, with a total of 36 electrodes, and provide up to four independent corrosion rates, depending on the type of probes used. Unfortunately due to spatial constraints only one physical probe (two sensors) at a time (18 electrodes maximum) could be used. Corrosion was monitored in either the open or crevice configuration during a single session.

A Model FH [(2)] silver/silver chloride reference electrode with hardwood junction was employed and connected to the multielectrode corrosion analyzer for the measurements of the corrosion potentials from each type of probe. A thermistor temperature probe was also connected to the corrosion analyzer for the measurement of the process temperature.

The process parameters were measured with the following electrodes:

- Durafet II [(3)] (ISFET) pH electrode
- Model 4905 [(3)] contact type conductivity probe
- Model DL5000 [(3)] dissolved oxygen probe

All the corrosion rates and process parameters were logged and displayed in real time using the multielectrode corrosion analyzer as data acquisition device connected to a panel computer running PC Anywhere v. 11.0 [(4)] installed so that computers in remote offices could communicate with this field computer and view the data online or download the data that were saved into the memory of the field computer.

The apparatus was set up and run continuously for over one year in our rolling facility and each of the above parameters measured, tabulated and compared.

System Installation in the Field

The probes were test fitted in a pipe adaptor or spool (Figure 3) in a laboratory prior to shipping to the mill for connection to the field system. All probes were located close to each other in the limited space of the spool and should see the same conditions at the same time. The conductivity probe was a flow through device. To insure that fluid was flowing through the conductivity cell during the measurement, the inlet cell was placed in a flow directed elbow per the manufacturer's specification.

[(2)]Electrochemical Devices Inc, (Albion, RI 02802-0031)

[(3)]Honeywell Instruments Sensing and Control, Ft. Washington, PA, 619034

[(4)]Symantec (Springfield, Oregon 97477)

The multielectrode corrosion analyzer was installed on a skid. The skid was placed on the open floor in the plant (Figure 4). The pipe adaptor containing the probes was installed in the coolant piping system in a place previously used for an expansion joint. The instrumentation was within 10 feet (3 m) of the probes (Figure 4). The pipe and skid frame initially were not grounded but later grounds to the buildings electrical system were installed.

Mathematic Modeling

To get to the root cause of corrosion and to facilitate process control, it was necessary to construct a crude mathematical model as the correlation of the individual data streams was inconclusive. JMP [(5)] software was used to derive the correlations between the localized corrosion rates and the system parameters, including conductivity, pH, corrosion potential, and dissolved oxygen concentration. These models are highly empirical and cannot be used as an exact mathematical prediction tool. The model was used to simply rank the order of importance of several parameters that have been measured over the course of this study.

RESULTS AND DISCUSSION

Localized Corrosion Rates and Process Parameters during an Operational Upsets

Figures 5 shows the carbon steel localized corrosion rate, conductivity, pH and temperature of the coolant system during a two month-monitoring period. The plant coolant system experienced a leak initially. Several linked events led to a gradual decrease in conductivity of the coolant after the leak was fixed. Acid was gradually introduced to the system when the conductivity reached 200 µSiemens/cm. The conductivity increased with the decrease in pH and reached 760 µSiemens/cm over a period of 5 days. There were some system upsets 5 days after the addition of the acid as evidenced by the sudden temperature drop. The upset was followed by an accidental addition of tap water into the system, which caused the decrease in temperature. The localized corrosion rate of carbon steel was low initially and started to increase when the pH suddenly decreased by one point and the conductivity passed the initial value (20 µSiemens/cm). When the tap water was accidentally added into the coolant system, the localized corrosion rate of carbon steel increased drastically from 150 µm/yr to 1400 µm/yr. Compared with the responses of the conductivity, the response of localized corrosion rate of carbon steel to the accidental addition of tap water underscores the significance of real time corrosion monitoring in identifying the operational upset. The coolant system conductivity and the carbon steel localized corrosion rate started to increase after the tap water was stopped and the upset condition was corrected.

Figure 6 shows the dissolved oxygen concentration in and the conductivity of the coolant, and the comparison between the localized corrosion rates of stainless steel (304L

[(5)]SAS Institute (Cary, NC, 27513)

SS) and carbon steel. The localized corrosion rate of the stainless steel was low (<0.1 µm/yr) until the acid addition. When the pH suddenly dropped, the localized corrosion rate of stainless steel increased to 0.7 µm/yr, but decreased gradually to 0.1 µm/yr, indicating that the stainless steel was passivated in the coolant system. The localized corrosion rate of stainless steel increased slightly from 0.06 to 0.3 µm/yr and remained at 0.3 µm/yr for only a short period of time when the untreated tap water was accidentally added into the coolant system. The localized corrosion rate of the stainless steel was lower than that of the carbon steel by a factor of 100 to 1000 during the entire monitoring period. These results favor the selection of stainless steel material for piping systems.

Figure 7 shows the localized corrosion rates and the corrosion potentials for the stainless steel and the carbon steel probes. The corrosion potentials for the carbon steel and stainless steel probes were about -0.41 and -0.28 V [vs. Ag/AgCl], respectively, before the addition of acid. The corrosion potential increased after the acid addition, showing the enoblization by the hydrogen ion.

Correlations of Localized Corrosion Rates with Process Parameters

The correlations between the measured localized corrosion rates and the system parameters, including corrosion potential, pH, conductivity, and dissolved oxygen concentration were modeled for both the carbon steel and the stainless steel materials. The equations derived from the real world data show each factor with coefficients and exponents weighting each and some are squared. This will signal which parameters are most important in these instances. It was necessary to break the system into high and low corrosion rates for each of the two metals.

For carbon steel, the following equations were derived:
High corrosion rate:

$$CR = -17785.850 - 79014.144CP - 5.700C - 80018.544\,CP^2 + 0.006C^2 \quad (1)$$

Low corrosion rate:

$$CR = 345.485 + 22.673CP + 0.141C - 55.824DO + 2.279\,DO^2 + 0.302CP \times C \quad (2)$$

In Equations 1 and 2, CR is the corrosion rate (µm/yr), CP is carbon steel corrosion potential (V), C is conductivity (µSiemens/cm), and DO is dissolved oxygen (ppm).

For stainless steel, the following equations were derived:
High corrosion rate:

$$CR = 3.724 + 19.893CP + 4.104\,CP^2 - 0.001C - 1.073CP \times DO - 0.223DO - 0.009\,CP \times C \quad (3)$$

Low corrosion rate:

$$CR = 0.021 + 0.053CP + 0.008pH - 0.0002C + 0.435CP^2 - 0.000001pH \times C + 0.0000003C^2 \quad (4)$$

.

In Equations 3 and 4, CP is the stainless steel corrosion potential (V), and others are the same as in Equations 1 and 2.

Figures 8 and 9 show the correlation between the model-predicted localized corrosion rates and the measured localized corrosion rates for carbon and stainless steel, respectively. The R^2 values are 0.91 for carbon steel and 0.74 for stainless steel. The temporal comparisons between the model-generated data and the real time data for carbon steel and stainless steel are given in Figures 10 and 11. In both cases, the shapes of the model-generated curves are in very good agreement with the real-time curves, showing that most of the time the model predicts reality.

Since high corrosion rate is of great importance in this situation, we will discuss those first. For both cases (carbon and stainless steel) the model showed that the corrosion potential was the most important factor followed by the solution conductivity.

The changes in conductivity were recorded simultaneously with the changes in corrosion potential and rate. This leads to immediate correlation of conductivity change to corrosion rate.

With stainless steel the dissolved oxygen played a minor role in the third term. In both cases with high corrosion rates the pH played a very negligible role in elevating the corrosion rate.

The corrosion potential was the most important factor when the corrosion rates were low. With carbon steel the conductivity is still important and dissolved oxygen becomes slightly more important. However pH now played a more important role with stainless steel followed by conductivity. We must point out that the low corrosion rates especially in the case of the carbon steel are up to 1000 times lower than the maximum rate observed in micrometers per year and even the high rate for stainless steel is 1000 times lower than the high rate for carbon steel.

Initially we saw excursions of corrosion current and did not see a correlation to conductivity or pH. Figure 12 shows data that was taken within the first few days of the installation. The spikes of current and therefore corrosion rate were temporally linked to drops of corrosion potential that were of a very rapid nature. Due to the large size of the system this was not attributed to a chemical phenomenon. In a plant setting these excursions could be due to several factors including electrical sources. After we isolated the spool and the skid the phenomenon were not observed again.

Crevice Corrosion Monitoring

In many mill situations crevice corrosion can be a large problem. System pipes are often located in very humid areas and there can be leaks from the coolant systems that sometimes drip on to the hangers used to support pipes. The hangers can allow the formation of a crevice against the external pipe walls. Moisture on the hanger (usually a plastic material), can slowly enter the crevice by capillary action. Often there are grooves inside the crevice that allow a considerable fluid build up may occur. Many times piles of metal salts can be seen on top of an active crevice.

The data from the combination probe (9 electrodes of stainless steel and 9 electrodes of carbon steel) with a crevice former (Figure2) are shown in Figure 13. The crevice corrosion rates for stainless steel and carbon steel inside the same crevice former were simultaneously gathered. When the crevice probe was inserted into the coolant system and brought on line, the localized corrosion rates between the two metals differed by a factor of about 10000, which is consistent with some of the data shown in Figure 6and 7. The corrosion potentials of the two metals were falling during this time, probably due to the depletion of oxygen inside the crevice. The carbon steel corrosion potential remained at a constant value (about -0.64 V [Ag/AgCl]) after initial decrease. The carbon steel localized corrosion rate varied from 10 to 100 µm/yr, and for most of the time, it was above 80 µm/yr.

The localized corrosion rate of the stainless steel was about 0.1 µm/yr initially and decreased slowly to about 0.03 µm/yr as the metal became passivated. However, three weeks after insertion, the stainless steel became completely depassivated, and the localized corrosion rate increased suddenly from 0.03 µm/yr to about 10 µm/yr. The depassivation of the stainless steel is also evidenced by the sharp decrease of the corrosion potential from -0.56 to -0.63 V [Ag/AgCl]. As the crevice corrosion of the stainless steel propagate, its localized corrosion rate continued to increase and even passed that of the carbon steel (>310 µm/yr) three weeks after the insertion of the probe in to the coolant system. The stainless steel probe did repassivate about two months later but this is not shown in the plot

Based the monitoring results for crevice corrosion, the use of stainless steel as a substitute for carbon steel is probably not the best choice and alternate solutions require removing the crevice altogether.

CONCLUSION

Corrosion (pitting and crevice) is a dynamic process changing in very short temporal sequences. The hypothesis was that an on-line meter was needed to understand corrosion in water based coolant systems. The use of an online instrument allowed coolant parameters that influence corrosion to be monitored and their importance assessed. The major factors are corrosion potential and conductivity. Understanding and quantifying corrosion phenomenon can provide valuable information for process control, process design, and material choices needed to prevent pitting and crevice corrosion in a

rolling mill operation. Controlling corrosion in a large system with an on-line feedback instrument is possible.

ACKNOWLEDGEMENTS

Sponsors: Kathy Tomaswick, Deborah Wilhelmy, Thomas Kasun and David Coleman all with Alcoa at ATC.

Technical Consulting: James Moran, Francine Bovard, with Alcoa at ATC, Lietai Yang, Corr Instruments.

REFERENCES

1. N.D. Budiansky, J.L. Hudson, J.R. Scully, "Origins of Persistent Interaction among Localized Corrosion Sites on Stainless Steel," Journal of the Electrochemical Society (2004), 151(4), B233-B243]

2. H. Cong, N. D. Budiansky and J. R. Scully, H. T. Michels, "Use of Coupled Electrode Arrays to Elucidate Copper Pitting as a Function of Potable Water Chemistry" CORROSION/07, paper no. 07392, Houston, TX: NACE, 2007

3. M. H. Dorsey, D. R. Demarco, B. J. Saldanha, G. A. Fisher, L. Yang and N. Sridhar, "Laboratory Evaluation of a Multi-Array Sensor for Detection of Underdeposit Corrosion and/or Microbially Influenced Corrosion," CORROSION/2005, paper no. 05371, Houston, TX: NACE, 2005

4. A. Anderko, N. Sridhar, L. Yang, S.L. Grise, B.J. Saldanha, and M.H. Dorsey, "Validation of a Localized Corrosion Model Using Real-Time Corrosion Monitoring in a Chemical Plant," Corrosion Engineering, Science and Technology (formerly British Corrosion J.), Vol. 40, pp.33-42, August, 2005

SUPPORTING DOCUMENTS

1. "NanoCorr Coupled Multielectrode Analyzers for Corrosion Monitoring and Corr Visual Software Instruction Manual" Version 2.0.0; May 2005, Corr Instruments LLC. San Antonio Texas

2. "DurafetII Industrial pH Electrode Series Operators Manual", 70-82-25-87; March 9, 2000, Honeywell Instruments Sensing and Control, 11 West Spring St., Freeport Illinois, 61032

3. "4905 Style Conductivity Cells for 04905 Series and DL4-5XX Direct Line Series Installation and Maintenance Manual", 70-82-25-18, June 2004, Honeywell

Instruments Sensing and Control, 1100 Virginia Drive, Fort Washington , PA , 619034

4. "DL5000 Dissolved Oxygen (D.O.) Probe Users Manual", 70-82-25-114, May 2002, , Honeywell Instruments Industrial Process Control, 1100 Virginia Drive, Fort Washington , PA , 619034

5. Electrochemical Devices web page @ http://www.edi-cp.com/

6. "Principles of Instrumental Analysis"; Douglas Skoog, 1985, Third Edition, Saunders College Publishing, West Washington Square, Philadelphia, PA 19105

FIGURES

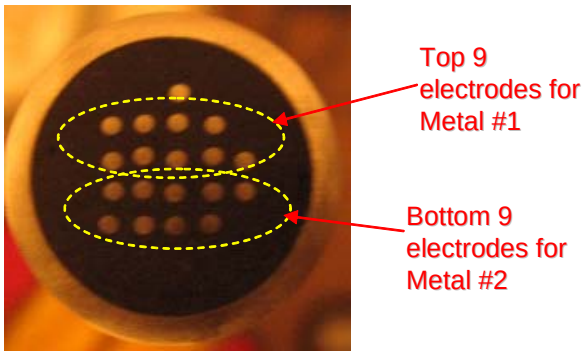

Figure 1. Typical combination coupled multielectrode probes.

Note: The electrodes for each metal are coupled independently during measurements. The electrode on the top is for indication of probe orientation only.

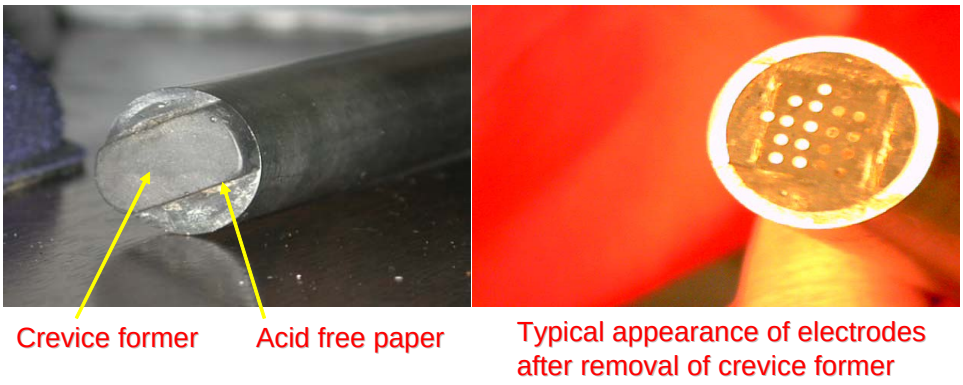

Figure 2. Typical creviced combination probes after service

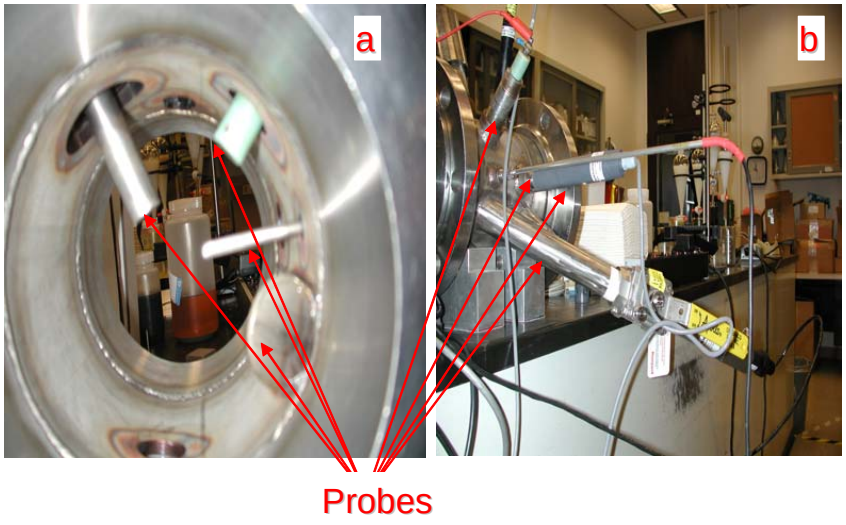

Figure 3. Internal (a) and external (b) views for probes installed in a pipe adaptor during the test fit in a laboratory

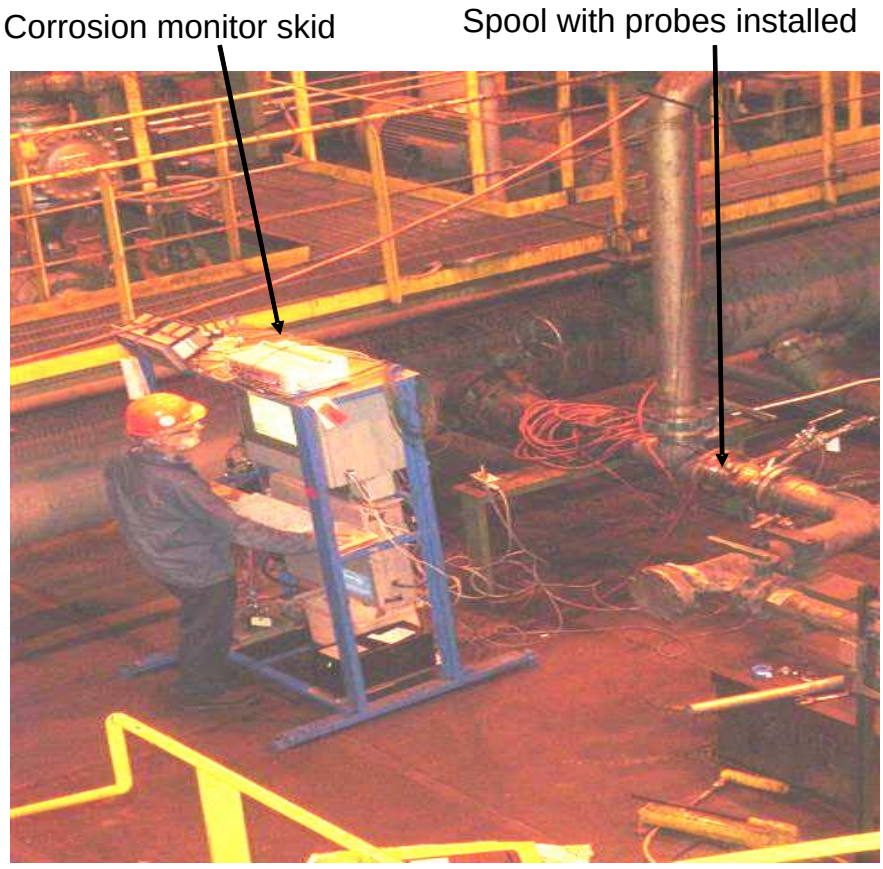

Figure 4. Instrumentation and probe installations in the field.

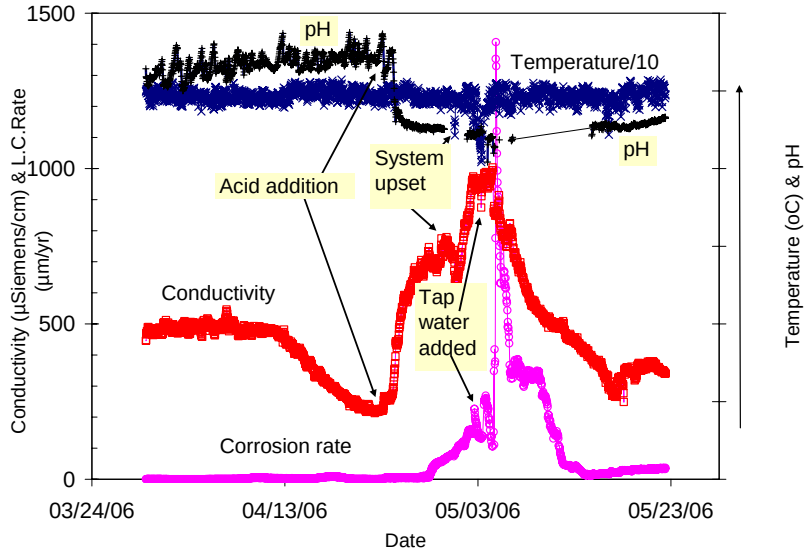

Figure 5. Responses of carbon steel localized corrosion rate, temperature, conductivity and pH to the upset condition during an excursion

Note: Temperature values were reduced by a factor of in the figure.

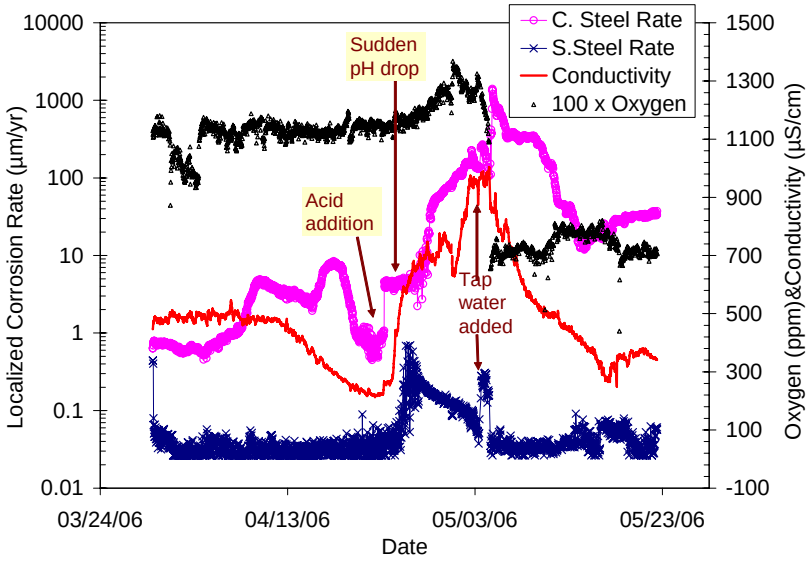

Figure 6. Comparison between the localized corrosion rates for carbon steel and stainless steel, and the dissolved oxygen and conductivity during the measurements. Note, the dissolved oxygen concentration (in ppm) was multiplied by 100 in the figure.

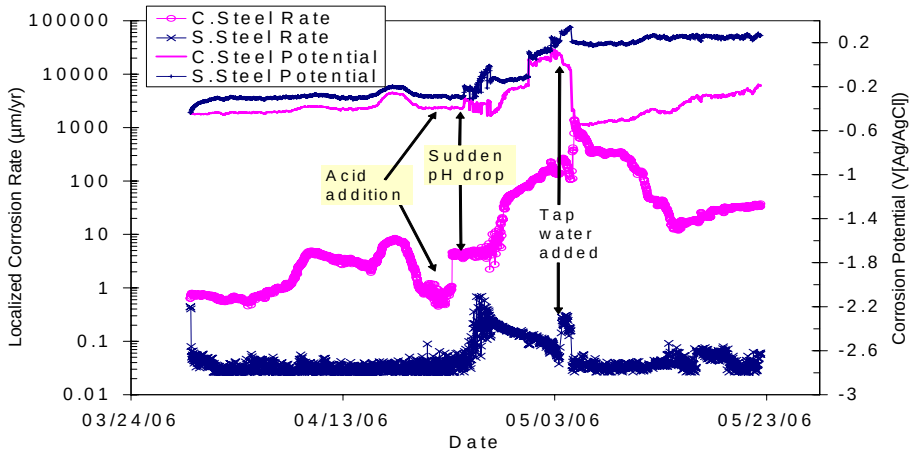

Figure 7. The responses of the corrosion potentials and localized corrosion rates for the stainless steel and carbon steel probes to the upset condition during the excursion

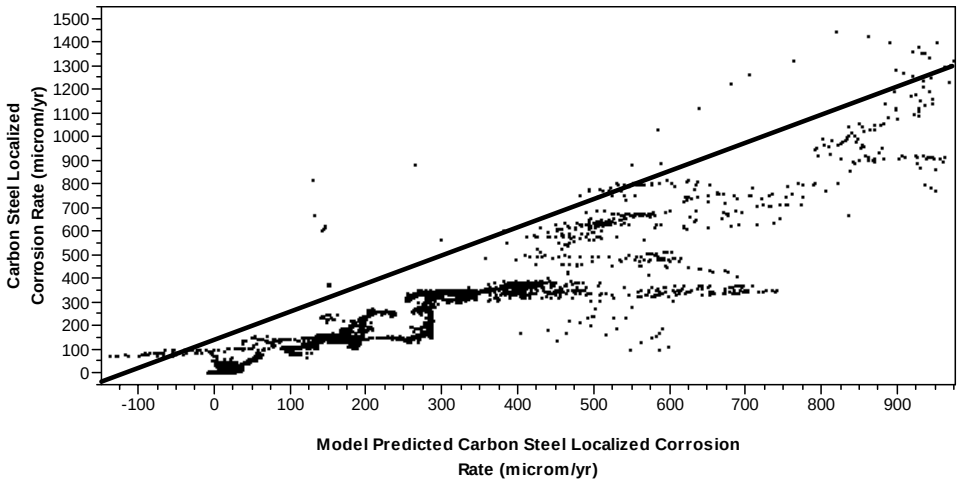

Figure 8. Correlation between model-predicted localized corrosion rates and the measured localized corrosion rates for carbon steel probe.

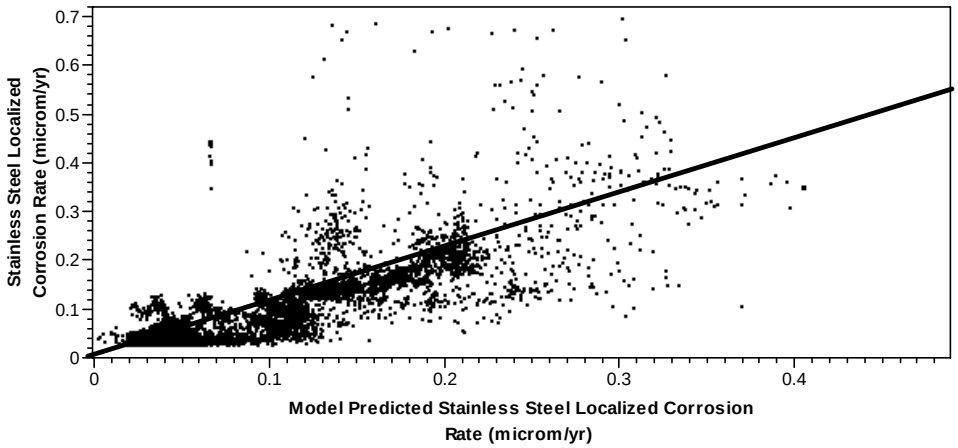

Figure 9. Correlation between model-predicted localized corrosion rates and the measured localized corrosion rates for the stainless steel probe

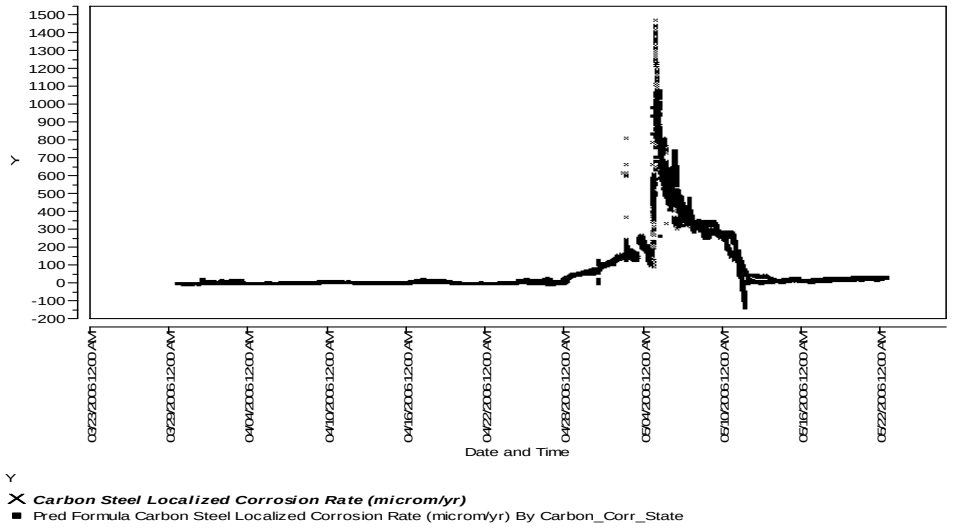

Figure 10. Temporal comparison between the model-predicted localized corrosion rates and the measured localized corrosion rates for the carbon steel.

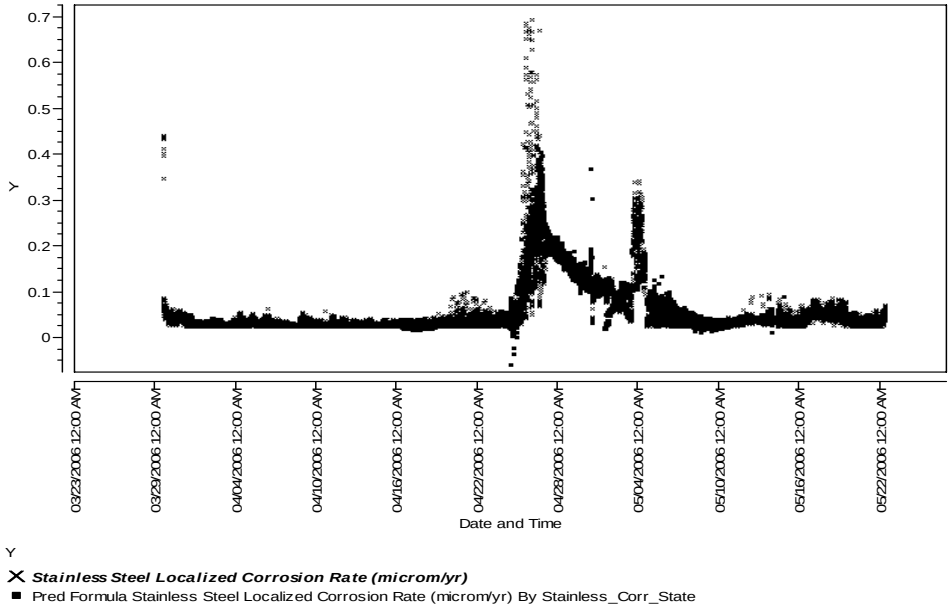

Figure 11. Temporal comparison between the model-predicted localized corrosion rates and the measured localized corrosion rates for stainless steel.

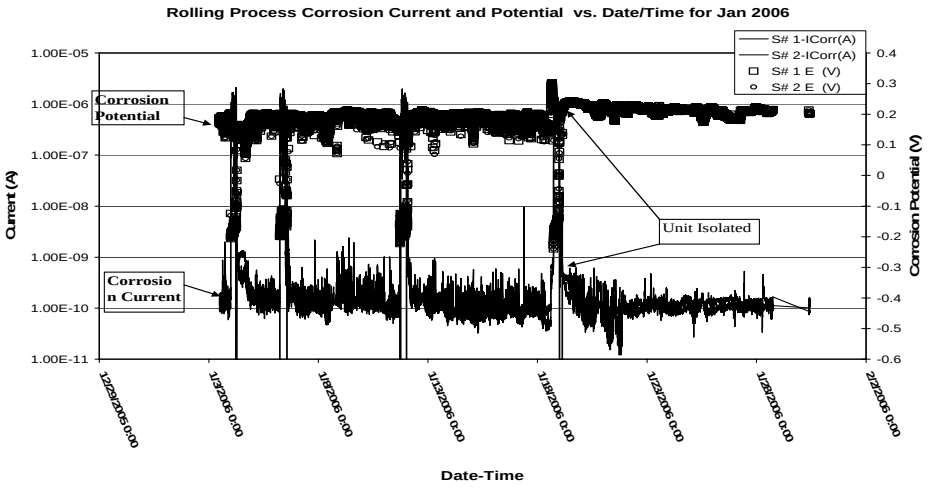

Figure 12. Corrosion current and potential during a one month period showing the effect of isolation on the corrosion response on the monitor.

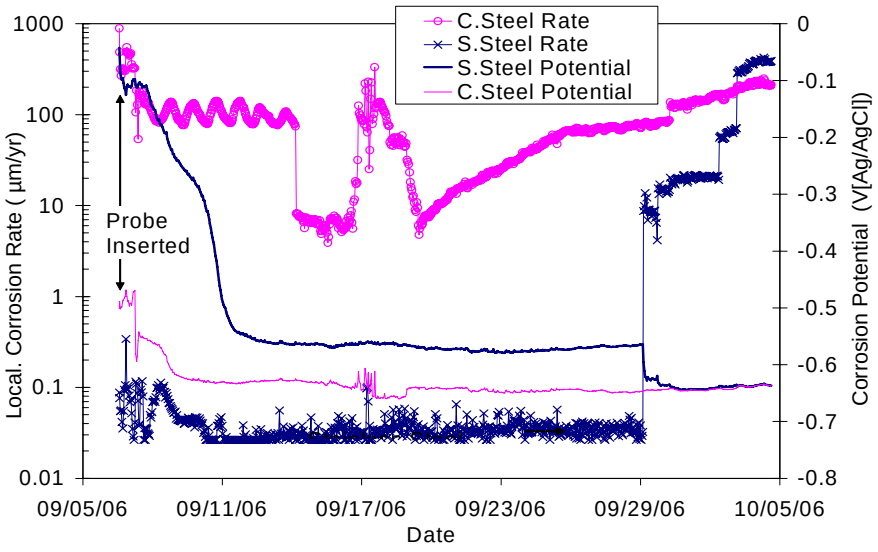

Figure 13. Localized corrosion rates and corrosion potentials from a combination creviced probe for carbon steel and stainless steel